Flight Validation of a Feedforward Gust-Attenuation Controller for an Autonomous Helicopter

Xilin Yang, Matt Garratt, and Hemanshu Pota

School of Engineering and Information Technology, University College, University of New South Wales, 2600, Canberra, Australia

Abstract

This paper presents a practical scheme to control heave motion for hover and automatic landing of a Rotary-wing Unmanned Aerial Vehicle (RUAV) in the presence of strong horizontal gusts. A heave motion model is constructed for the purpose of capturing dynamic variations of thrust due to horizontal gusts. Through construction of an effective gust estimator, a feedback-feedforward controller is developed which uses available measurements from onboard sensors. The proposed controller dynamically and synchronously compensates for aerodynamic variations of heave motion, enhancing disturbance-attenuation capability of the RUAV. Simulation results justify the reliability and efficiency of the suggested gust estimator. Moreover, flight tests conducted on our Eagle helicopter verify suitability of the proposed control strategy for small RUAVs operating in a gusty environment.

Keywords:
rotary-wing unmanned aerial vehicle; feedforward controller; gust estimator; gust attenuation;

1. Introduction

RUAVs are suitable for a variety of applications such as surveillance and reconnaissance, search and rescue of dangerous areas such as volcanoes. There is also a growing desire to operate RUAVs from ships at sea which introduces new challenges owing to the adverse turbulent gusts over the flight deck and the ship motion due to waves. Operational flexibilities, including vertical take-off and landing capability, hover at a desired height, longitudi-

nal and lateral manoeuvre, etc., make the RUAV an indispensable platform to perform such operations.

The main challenge in fulfilling maritime landing tasks results from the complicated aerodynamic environment, which consists of wave-excited movement of the ship deck and horizontal turbulent gusts. There are notable variations of ship airwake due to ship's superstructure and ambient surface conditions [1]. Besides, the RUAV operates in a partial ground effect condition where both the magnitude of the rotor flow and the inflow distribution over the rotor disk vary greatly [2]. This phenomenon results in a considerable change in the aerodynamic loading of the rotor system, which affects the RUAV control margins, autopilot workload and power margins [3]. Therefore, dynamic performance of the RUAV is deteriorated, and pure feedback driven controllers fail to stabilize the heave motion. This difficulty justifies the need for a controller with gust-attenuation properties.

The gusts imposed on a RUAV mainly come from the ship airwake, which is governed by a variety of factors such as the geometry of the ship superstructure, intensity and relative direction of the natural wind, free-stream turbulence, and interactions of the ambient environment (sea motion and weather conditions, etc.) with ship dynamics [4, 5]. Typically, the interactions of atmospheric winds with the ship superstructure leads to substantive flow separations and the formation of violent vortices over the landing deck. Ship airwake modeling using proper approaches has been subject to extensive investigations in a considerable number of papers, and significant efforts, including theoretical analysis and experimental research, have been made to deal with various combinations of ships and helicopters [6, 7, 8, 9]. In general, ship airwake can be modeled using the Computational Fluid Dynamics (CFD) data or the deterministic gust models. The CFD approach is suitable for both steady-state and unsteady-state (time-accurate) ship airwake scenarios [6, 8, 10]. Also, implementation difficulties need to be considered, as the CFD method requires dealing with large quantities of data, making it challenging for real-time computation [7]. In our case, we assume that detailed ship deck configuration is unknown.

At present, numerous papers have addressed the effect of gusts on fixed-wing aircraft. Based on a linearized model, Aouf *et al.* [11] design an H_∞ controller to reduce effect of gusts on aircraft vertical motion using a Dryden gust model. Buffington *et al.* [12] present a minimal-order robust controller to attenuate lateral gusts of an aircraft. A spatial sliding mode controller is proposed by Jackson *et al.* [13], in which wind disturbances with known

bounds are explicitly considered in their UAV model. However, it may be challenging to set upper bounds on wind gusts in real scenarios due to the complex mechanism of turbulence. In contrast, investigations on helicopters in a turbulent environment have received less attention than their fixed-wing counterparts. Recently, Cheviron *et al.* [14] propose a robust guidance and control scheme for an autonomous helicopter in the presence of wind gusts. A high-gain observer is used to reconstruct the unknown inputs, and time derivatives of the inputs are assumed to be uniformly bounded. Maritini *et al.* [15] address control of a model-scale helicopter under wind gusts. The disturbances in their paper are vertical wind gusts with typical levels less than 1 ms^{-1}. In our case, we concentrate on horizontal gusts with a typical level of 10 ms^{-1}, since the main factor influencing thrust in hover comes from horizontal gusts, particularly close to the ground where the vertical gust component is near zero.

The present study begins with establishing a dynamic relationship between horizontal gusts and thrust. A gust estimator is constructed to estimate horizontal gust levels in the presence of sensor errors and measurement errors. A feedback-feedforward controller is presented to compensate for side effects from horizontal gusts. Simulation results demonstrate that our gust estimator can estimate gust levels, and the proposed controller is able to attenuate impact of the horizontal gusts and stabilize heave motion of the RUAV in a gusty environment. Moreover, experimental tests have confirmed the validity of this method.

This work is based on available data collected from a small 8 kg RUAV, known as the *Eagle* (see [16] for platform description). The Eagle helicopter and its avionic systems are shown in Fig. 1 and Fig. 2. The Eagle is a fully instrumented and electrically propelled helicopter which has been used to demonstrate autonomous hover control using neural networks [17], backstepping [18] and classical control theories [19]. The Eagle is very susceptible to wind gusts owing to its small size. The algorithms were tested on the Eagle as a precursor to work with larger helicopters, such as the Yamaha RMAX, which we are adapting for operations from ships [20].

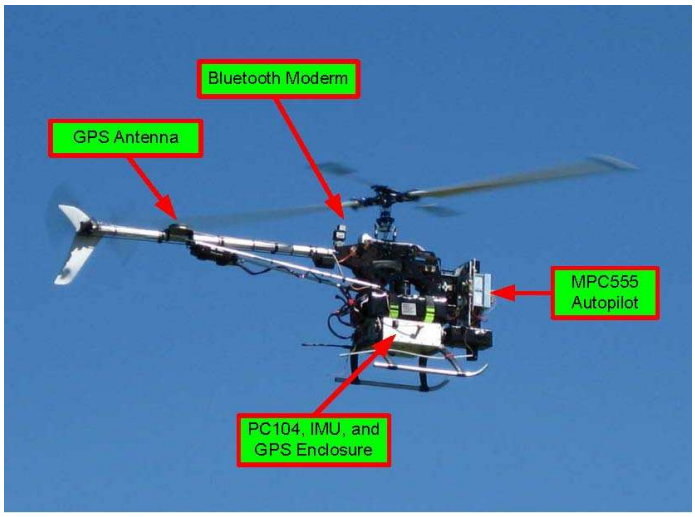

Figure 1. UNSW@ADFA Eagle helicopter in flight

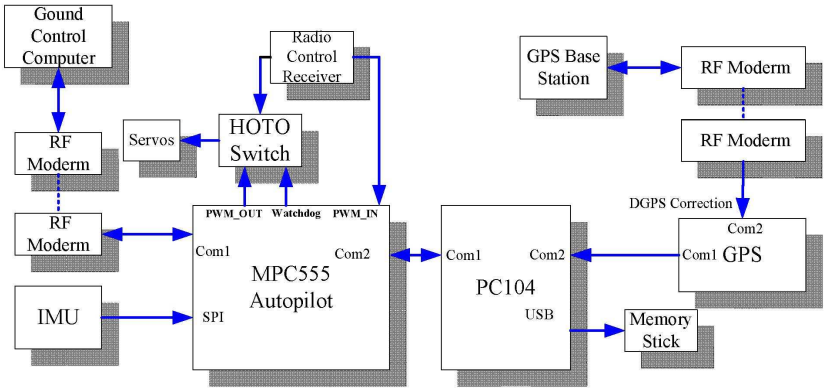

Figure 2. Eagle avionic architecture

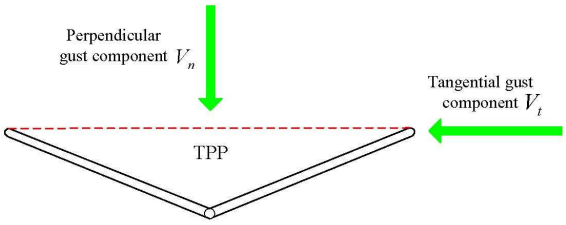

Figure 3. Decomposition of gusts acting on the main rotor

2. Heave motion dynamics under atmospheric disturbances

2.1. Heave motion dynamics of the RUAV

Heave motion dynamics of the RUAV can be described as:

$$\dot{w} = \frac{mg - T_{mr}}{m}, \tag{1}$$

$$\dot{z} = w. \tag{2}$$

Here, w is vertical velocity, z vertical distance, and m mass of the RUAV. The main rotor thrust T_{mr} is vulnerable to fluctuations when gusts V_t^2 occur. To design a proper controller reducing the detrimental effect, we begin with analysis of horizontal wind gusts, and then investigate thrust variations due to the gusts.

The oncoming air stream velocity V_∞ consists of two components, V_t and V_n shown in Fig. 3, which are tangential and perpendicular to the tip path plane (TPP),

$$V_\infty^2 = V_t^2 + V_n^2. \tag{3}$$

The relationships between air stream velocity components and velocity components of the RUAV are described by (pp.19 [21],[19]):

$$V_t^2 = u^2 + v^2, \tag{4}$$

$$V_n = (a_1 + i_s)u - b_1 v - w. \tag{5}$$

Here, designations u, v and w are velocity components of the RUAV along body reference coordinates. Symbols a_1 and b_1 are longitudinal and lateral

flapping, respectively. The main rotor shaft angle is denoted by i_s. The body reference is defined such that the origin is located in the center of gravity of the RUAV with x-axes pointing positive to forward, y-axes sideways, and z-axes downwards.

Since flapping angles rarely exceed 10 degrees during normal flight [19, 22], compared with the perpendicular component V_n, it is seen from Eq. (4)-(5) that the tangential component V_t is dominant in a gusty environment, and referred to as gusts in the following context. The perpendicular component V_n can be approximated by vertical velocity w with opposite sign due to the small quantities of $(a_1 + i_s)$ and b_1 $(a_1, b_1 < 5^0, i_s < 10^0)$ ([19, 22]).

The main rotor thrust (T_{mr}) in a conventional helicopter is generally controlled using the *collective pitch* control with symbol θ_{col}. The collective pitch controls the mean angle of attack of the rotor blades around the rotor disk and hence the lift that is generated. Referring to [19, 23], the thrust equation employed in our case takes the following form:

$$T_{mr} = \frac{\rho a N_b A_b (\Omega R)^2}{2} [\frac{\theta_{col}}{3}(1 + \frac{3V_t^2}{2\Omega^2 R^2}) - \frac{V_n + V_i}{2\Omega R}], \tag{6}$$

where ρ, a, and N_b are air density, lift curve slope of main rotor blade, and the number of blades. A_b is blade area, Ω is angular speed of the main rotor, R is main rotor radius, and V_i is induced velocity of the air through the main rotor.

Another formula is needed to solve for the unknowns V_i and T_{mr}. We use Glauert's formula [19, 23, 24]:

$$V_i^2 = \sqrt{(\frac{\hat{V}^2}{2})^2 + (\frac{T_{mr}}{2\rho A_d})^2} - \frac{\hat{V}^2}{2}, \tag{7}$$

where

$$\hat{V} = \sqrt{V_t^2 + (V_n + V_i)^2}, \tag{8}$$

and $A_d = \pi R^2$ is rotor disk area. A resultant velocity $\hat{V}$ is employed. The formula is reported to be true for all loading distributions on occasions when high speed gusts are encountered [24]. Equations (6)-(8) are coupled nonlinear equations which must be solved numerically to find the main thrust.

3. Development of the gust estimator

3.1. Design of a filter to reduce sensor errors

In our project, eight elastomeric isolators are installed to prevent the autopilot and inertial sensors from damaging vibration [19]. However, physical isolation of accelerometers cannot eliminate vibration effects to an acceptable level, and acceleration sensors are frequently subject to noise yielded by vibration. Based on measurements taken on our RUAV, we simulate a periodic vibration in the accelerometer taking the form of $A_m \sin(\omega_m t)$ with the amplitude A_m of 2 ms^{-1} and frequency ω_m of 20 Hz. Also, zero drift is an intrinsic error in the low-precision sensors typically used in small unmanned helicopters. Moreover, measured vertical velocity contaminated by sensor errors will also impair performance of the gust estimator.

Due to the contamination from different onboard errors, measurements cannot be directly utilized to develop the gust estimator. Feasible filters are required to extract desired signals. Therefore, Moving Average Filters (MAF) are employed to smooth out the measurements taking the following form

$$c_{af}(i) = \frac{1}{N_0} \sum_{k=0}^{N_0-1} c_{bf}(i-k), \tag{9}$$

where c_{bf} can be noisy a_z, w, or θ_{col}, and c_{af} can be filtered acceleration a_{z_f}, velocity w_f, or collective pitch θ_{col_f}. N_0 denotes the number of neighboring data points. The MAFs will serve when enough data points N_0 are stored in computer memory.

3.2. Implementation of the proposed gust estimator

It can be obtained from Eq. (6) that V_i can be expressed in terms of gusts V_t^2

$$V_i = 2\Omega R[\frac{\theta_{col}}{3}(1 + \frac{3V_t^2}{2\Omega^2 R^2}) - \frac{T_{mr}}{B_t}] - V_n, \tag{10}$$

where $B_t = 0.5\rho a N_b A_b (\Omega R)^2$.

The bisection search method is used to solve the nonlinear equation. We start by re-writing the induced velocity equation as

$$f(V_t^2) = \sqrt{\frac{[V_t^2 + (V_n + V_i)^2]^2}{4} + (\frac{ma_z}{2\rho A_d})^2} - \frac{V_t^2 + (V_n + V_i)^2}{2} - V_i^2. \tag{11}$$

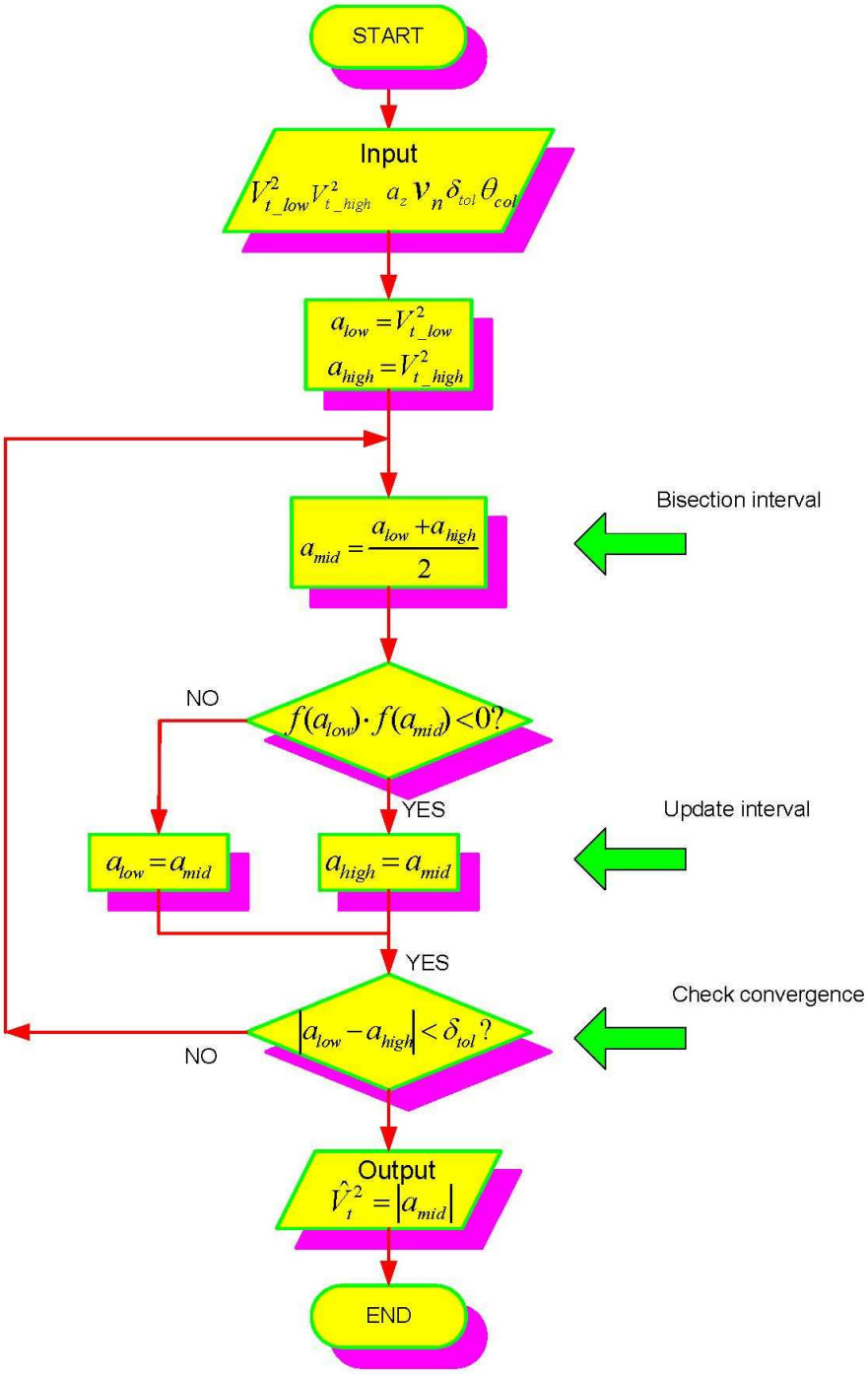

Figure 4. Flow chart for implementation of bisection algorithm

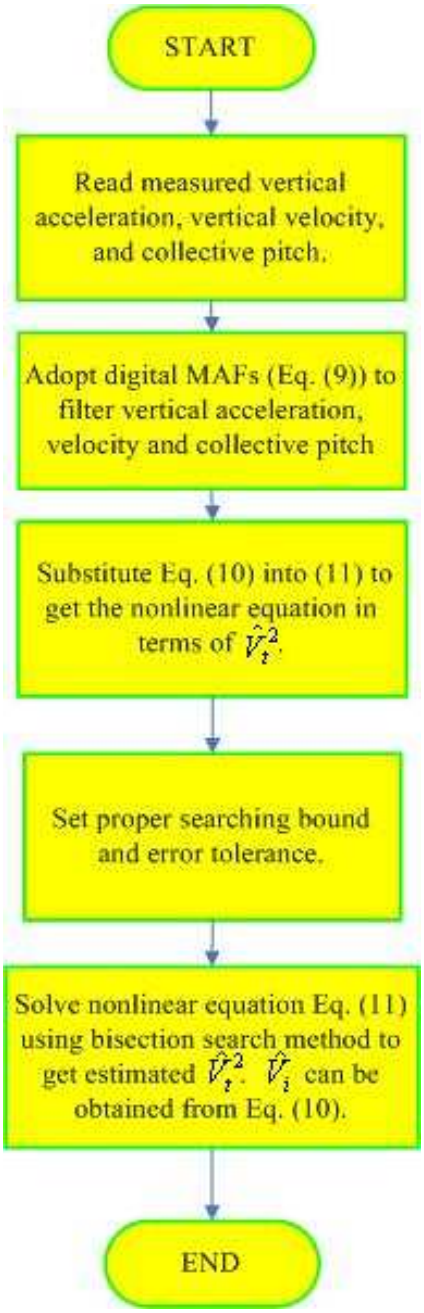

Figure 5. Flow chart for implementation of the gust estimator

Substituting Eq. (10) into Eq. (11) leads to an equation with one unknown variable V_t^2, and it can be estimated using the bisection algorithm as depicted in Fig. 4. The bisection algorithm begins with a proper choice of searching interval $[a_{low}, a_{high}]$ which guarantees a reasonable solution $\hat{V}_t^2$ is enclosed. Then the bisection point is calculated $a_{mid} = \frac{a_{low}+a_{high}}{2}$. If $f(a_{low})$ is of opposite sign to $f(a_{mid})$, then the solution must lie within the smaller interval $[a_{low}, a_{mid}]$, and the upper bound a_{high} is reset to a_{mid}. In contrast, the possibility that $f(a_{low})$ is the same sign as $f(a_{mid})$ indicates the lower bound a_{low} should be replaced with a_{mid}. Therefore, the algorithm iteratively bisects the intervals, generating a sequence of subintervals that guarantee to converge to a proper solution [25]. The bisection algorithm keeps going until the length of the subinterval is within the predefined error tolerance δ_{tol}. Essentially, it takes 24 iterations to converge within an error tolerance of $1e{-}4\ m^2/s^2$. A C-file S-function block in MATLAB/SIMULINK was implemented to calculate $\hat{V}_t^2$ and induced velocity $\hat{V}_i$.

The procedure for estimating the gust levels $\hat{V}_t^2$ and corresponding induced velocity $\hat{V}_i$ is shown in Fig. 5. Firstly, MAFs are adopted with proper window width to filter measured acceleration, velocity, and collective pitch. Afterwards, through setting suitable searching scope and error tolerance, we can solve nonlinear equations to acquire estimated gusts $\hat{V}_t^2$ and induced velocity $\hat{V}_i$ using the bisection search method.

4. A gust-attenuation controller for heave motion of a RUAV

The proposed feedback-feedforward controller consists of two parts. The first part is to design a Proportional Derivative (PD) controller achieving satisfactory performance when no gusts occur; the second part, which is based on the estimation of the gusts $\hat{V}_t^2$ and induced velocity $\hat{V}_i$, aims to calculate the required collective pitch to compensate for dynamic variations when gusts occur.

The architecture of the disturbance-attenuation control strategy is illustrated in Fig. 6. Firstly, the RUAV heave dynamics are modeled by Equations (1)-(2) in consideration of gusts disturbance. In the gust estimator block, feasible MAFs are constructed to extract true states from the noisy measurements. Here, window widths of MAFs are 0.4 s for measured w, a_z, and θ_{col}. Then, these filtered variables serve as inputs to the gust estimator, and estimated gusts $\hat{V}_t^2$ and induced velocity $\hat{V}_i$ are acquired by the estimation procedure shown in Fig. 5.

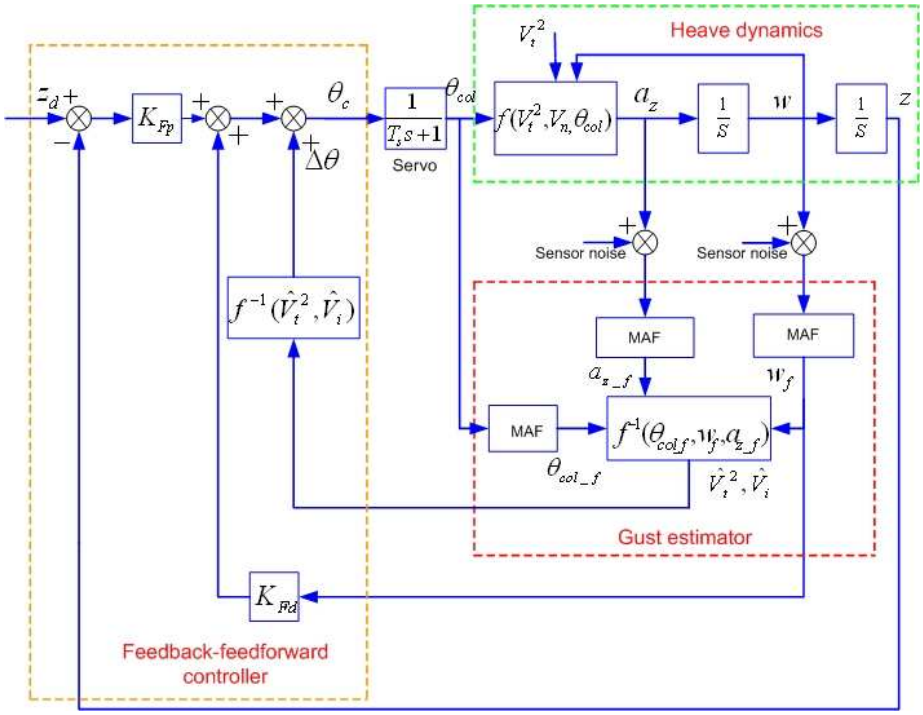

Figure 6. Block diagram of the proposed control strategy

Our ultimate purpose is to calculate the required collective pitch $\Delta\theta$, and add it to the nominal collective pitch (collective pitch required when no gusts occur) to compensate for dynamic variations. The feedback-feedforward control law θ_c is in the form of:

$$\theta_c = K_{Fp}(z_d - z) + K_{Fd}w + \Delta\theta. \tag{12}$$

Here, z_d is the desired height. The introduction of $\Delta\theta$ aims to indicate how much collective pitch deviates from the nominal value due to the oncoming gusts. By adding the $\Delta\theta$ to the control command, the helicopter can synchronously compensate for gust effects and can be stabilized at the desired height. The collective pitch offset $\Delta\theta$ is calculated by:

$$\begin{aligned}\Delta\theta &= \theta|_{V_t^2=V_g} - \theta|_{V_t^2=0} \\ &= \frac{3(\frac{T_{mr}}{B_t} + \frac{\hat{V}_{ig}+V_{ng}}{2\Omega R})}{1+\frac{3\hat{V}_t^2}{2\Omega^2R^2}} - 3(\frac{T_{mr}}{B_t} + \frac{\hat{V}_{i0}+V_{n0}}{2\Omega R}).\end{aligned} \tag{13}$$

Here, symbol $\theta|_{V_t^2=V_g}$ represents the required collective pitch to make the RUAV stable when gust levels are V_g, and the required collective pitch when no gusts occur is denoted by $\theta|_{V_t^2=0}$. Coefficient $\hat{V}_{ig}$ and V_{ng} denote the estimated induced velocity and vertical component of air stream (V_{ng} is approximated by w with opposite sign) when $\hat{V}_t^2 = V_g$, and $\hat{V}_{i0}$ and V_{n0} when no gusts occur. As we are concerned with the hover state, vertical components V_{ng} and V_{n0} in Eq. (13) can be set to 0, and thrust T_{mr} is replaced with weight W of the RUAV. Therefore, Equation (13) becomes

$$\Delta\theta = \theta|_{V_t^2=V_g} - \theta|_{V_t^2=0} = \frac{3(\frac{W}{B_t} + \frac{\hat{V}_{ig}}{2\Omega R})}{1+\frac{3\hat{V}_t^2}{2\Omega^2R^2}} - 3(\frac{W}{B_t} + \frac{\hat{V}_{i0}}{2\Omega R}). \tag{14}$$

It is seen that the required collective pitch $\Delta\theta$ to make the RUAV stable can be obtained, provided the estimates of $\hat{V}_{ig}$ and $\hat{V}_t^2$ are available, which are the outputs of the gust estimator. The resultant $\Delta\theta$ will be combined with the PD controller to increase gust-attenuation capacity of the RUAV.

5. Simulation results

In this section, overall performance of the proposed controller, in combination with a comprehensive evaluation of the gust estimator, is tested

using the heave motion model based on simulation parameters consistent with those employed in real applications. Operational limits in the collective pitch ($1^o < \theta_{col} < 10^o$) and the rate limit in servo dynamics ($|\dot{\theta}_{col}| < 20^o/s$), are taken into account. In our RUAV, the control commands are implemented using the Pulse Width Modulation (PWM) signals, and there is an approximate linear relationship between collective pitch commands and PWM signals, which can be computed after calibrations.

To acquire a reliable performance evaluation of the gust estimator, horizontal gusts are constructed using the Dryden turbulence model by passing white noise through shaping filters in longitudinal and lateral directions [26]. It should be clarified that no stochastic properties of the gusts are used to design the gust estimator, and the validity of the gust estimator is not restricted to specific gust conditions. The Dryden models are employed to generate typical gusts with representative properties so that they can be used to test the gust estimator.

Numerous simulations have been carried out for possible oncoming gusts, and the performance of the gust estimator is illustrated in Fig. 7. All the simulations are implemented for 100 s with sampling time of 0.02 s. The survival possibility of the RUAV is threatened by strong unpredictable gusts, especially on occasions when gust variations resulting from turbulence change take place with a high speed, and persist in duration. Also, the RUAV is vulnerable to frequent changing gusts. Consequently, our gust estimator is tested in such challenging environments. Two typical cases are tested in Fig. 7. Comparison results show that the estimated gusts are close to the gusts generated by software (assumed to be real gusts), with maximum estimation errors of 4.55 ms^{-1} and 2.45 ms^{-1}, separately.

Several quantitative specifications are employed to evaluate performance of estimated $\hat{V}_t^2$, which consist of maximum relative estimation error ς, and estimation capacity factor η. The index ς is used to check maximum relative estimation error, and η aims to evaluate overall estimation performance. The definition of these specifications are listed as follows:

$$\varsigma = \frac{\max_i |V_t^2(i) - \hat{V}_t^2(i)|}{V_t^2(i)}, \tag{15}$$

$$\eta = 20 \log_{10} \frac{\sqrt{\Phi}}{\max_i |V_t^2(i)|}, \tag{16}$$

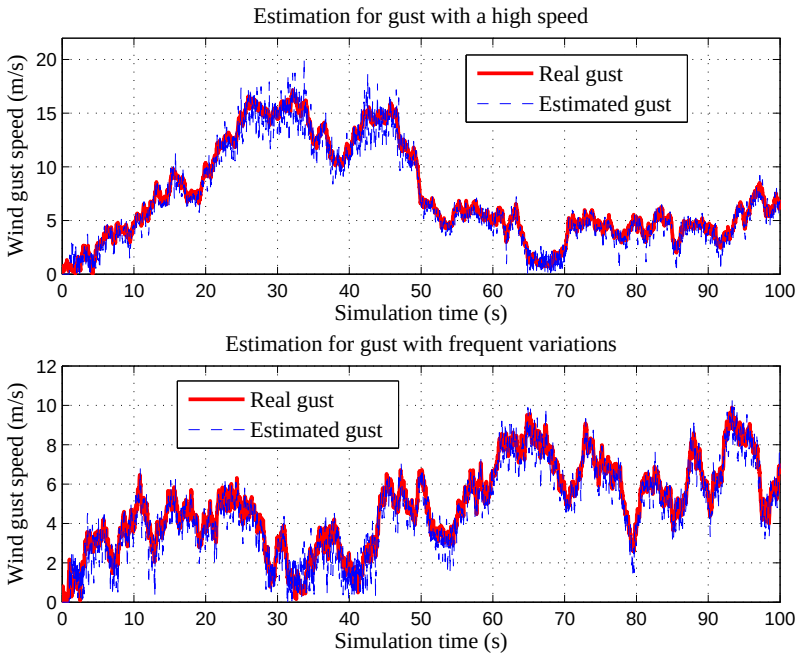

Figure 7. Estimation of gust variations

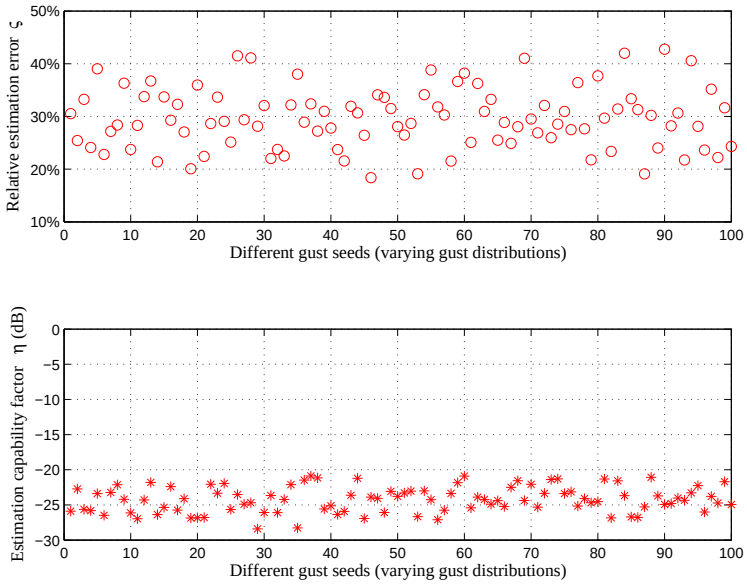

Figure 8. Performance evaluation of the proposed gust estimator

where mean squared error Φ is defined by

$$\Phi = \frac{1}{N}\sum_{i=1}^{N}[V_t^2(i) - \hat{V}_t^2(i)]^2. \tag{17}$$

As is shown in Fig. 8, maximum relative estimation error ς of $\hat{V}_t^2$ is consistently within 50% of V_t^2, which is satisfactorily accepted in our scenario. Also, the estimation capacity factor η of $\hat{V}_t^2$ remains less than $-20\ dB$, which indicates that a mean estimation error within 10% of the desired gusts V_t^2 can always be obtained.

Comparisons on induced velocity are displayed in Fig. 9 for the two typical gusts mentioned before. Although there are some small deviations at the initial stage, our estimator can consistently give good estimation of induced velocity. As is depicted in Fig. 10, the resultant collective pitch command θ_{col} can effectively compensate for the gusts, and the RUAV can

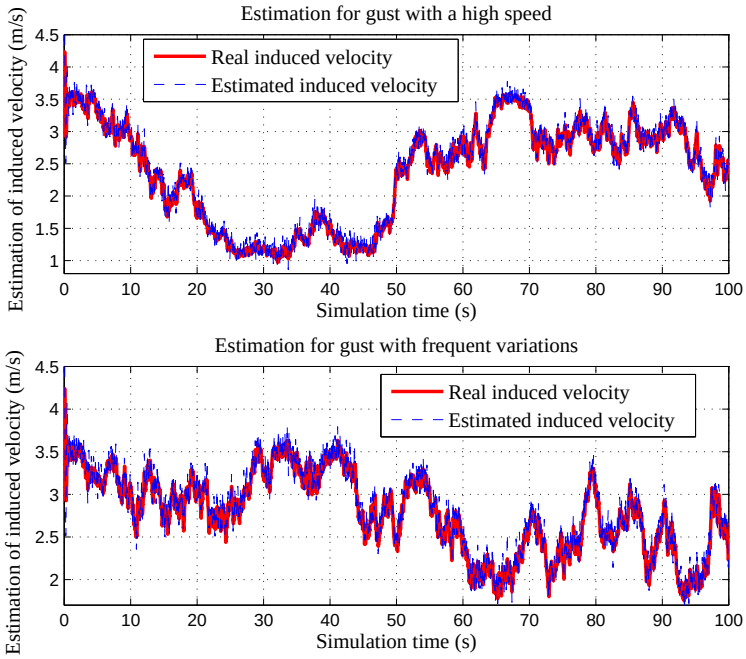

Figure 9. Estimation of induced velocity

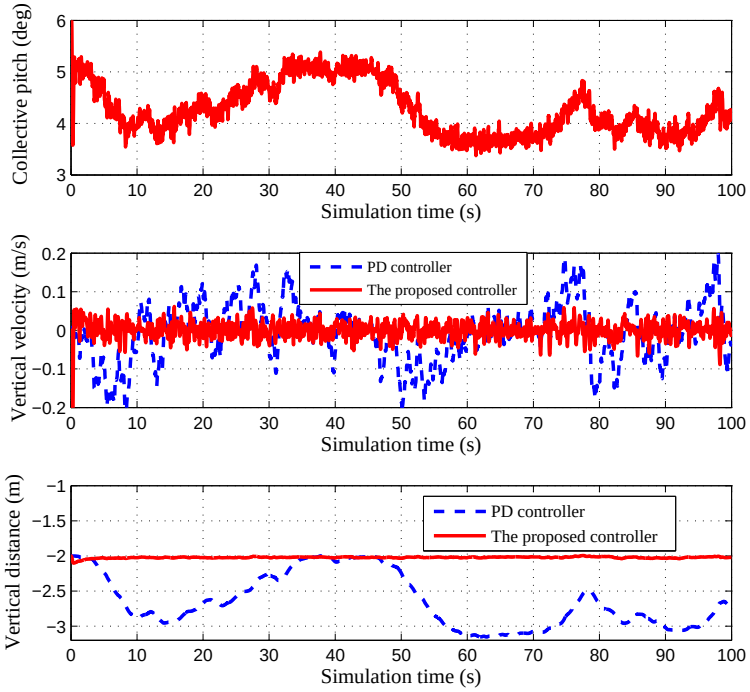

Figure 10. Control and dynamic response of RUAV heave motion

hover at the desired height stably ($-2\ m$). Here, control gains K_{Fp} is 0.022, and K_{Fd} is 0.045. It can be seen that vertical velocity converges quickly to zero, and is not subject to fluctuations. It is evident in Fig. 10 that the proposed controller can efficiently compensate for heave motion once random gusts occur when compared with a PD controller. Therefore, our control strategy ensures stable dynamic response of the RUAV in a windy environment, so that the RUAV hovers safely at a desired altitude over the ship deck before landing on an assigned location.

6. Flight test results

A series of experiments have been conducted to evaluate the performance of the gust estimator for integration with the feedback-feedforward controller. The small size and remote-control capability make the Eagle helicopter an ideal platform for flight validation. Parameters of the Eagle are given in Appendix.

The initial field tests showed that the measurement noise in acceleration, velocity, and collective pitch deteriorates the performance of the gust estimator. This necessitates design of MAFs with proper window width. The choice of the width of MAFs should guarantee effective removal of measurement noise, and reduce oscillations in the estimated thrust. Therefore, the window width for the three average filters are increased to 20 points after a few flight trials.

The collective pitch servo receives the anticipated control command, and drives servo horns to implement desired activities through linkages. Control signals generated by the MPC555 autopilot are sent to the digital collective pitch servo in the form of PWM signals at an update rate of 50 Hz. The PWM sequences repeat every 20 milliseconds (ms) with the minimum duty cycle of 1 ms and the maximum of 2 ms.

The field test began with finding out the proper trim collective pitch under the particular flight conditions when flight tests were conducting, then the trim collective were kept unchanged for the remaining tests. Since the main purpose is to control collective pitch due to its vulnerability to wind gusts, it is reasonable to control tail rotor, throttle, aileron, and elevator channels individually using the pure PD controllers. This would reduce experimental complexities when tuning control gains for a specific control channel. During flight tests, the Eagle helicopter was initially brought to a safe flight condition using the manual control mode, which is necessary for potentially

hazardous experiments requiring successive attempts. Also, special attention were paid to the flight close to the ground as slight variations in collective pitch would lead to rapid changes in height. Therefore, handover to the automatic mode is forbidden to prevent unexpected transitional responses resulting in dynamic oscillations which would cause crash of the helicopter. Handover to the automatic mode was activated after the helicopter reached to a desired height, and the autopilot micro-controller started sending control signals used for closed-loop flight tests. The automatic control mode was running for a few seconds to achieve smooth transition responses before the feedforward controller was switched on. Once turned on, the feedforward part operated in parallel with the feedback controller to produce the desired amount of collective pitch.

The experimental results from the flight test conducted on a windy day with the gust speed of approximately 20 km/h are listed below. The gust speed was known by checking official web site of the Australian Bureau of Meteorology on that day [27]. The flight test results shown in Fig. 11 indicate that the helicopter experienced significant oscillations in height when only controlled by PD controller. The oscillations reduced greatly after the feedforward controller was initiated at 52.5 s, and the height remained around 6.9 m under wind gusts. After the feedfoward controller was turned on, there were transitional response which last for about 16.5 s. The transition is revealed in vertical velocity shown in Fig. 12. Afterwards, the velocity tended to experience smaller changes. It is seen from Fig. 13 that the MAFs extracted the acceleration effectively from the noisy measurements. Low limit was set in the gust estimator code in case that the gust levels are too small to be detected. As is shown in Fig. 14, it took around 10 seconds for the gust estimator to effectively estimate the real gust levels owing to the transient response in collective pitch and ground effect during the take-off phase. The collective pitch commands are depicted in Fig. 15. It is noticed that the rate of change of collective pitch increased greatly after 52.5 s, which was introduced by the rapid change of collective pitch correction commands produced by the feedforward controller. The corresponding pitch correction commands are shown in Fig. 16.

7. Conclusion

In this paper we concentrate on building a feasible gust estimator for controlling heave motion dynamics of a RUAV. Based on construction of

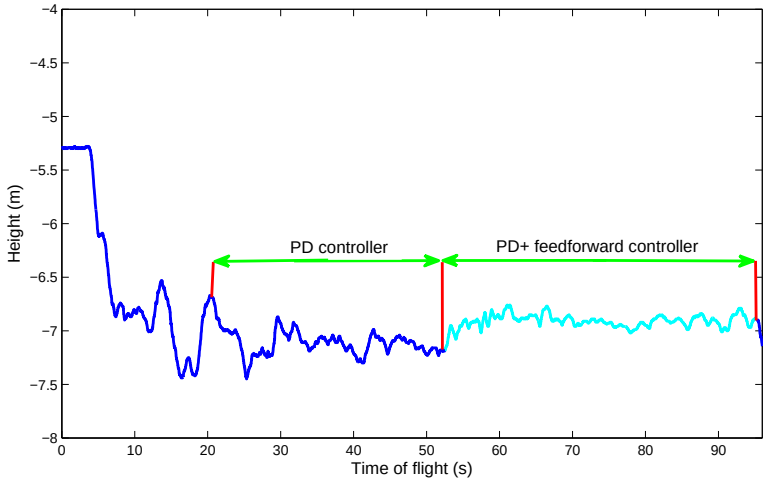

Figure 11. Height in the flight test

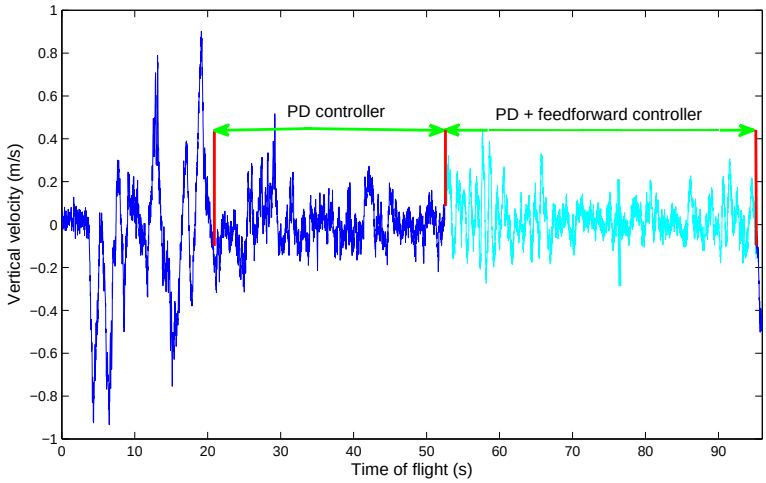

Figure 12. Vertical velocity in the flight test

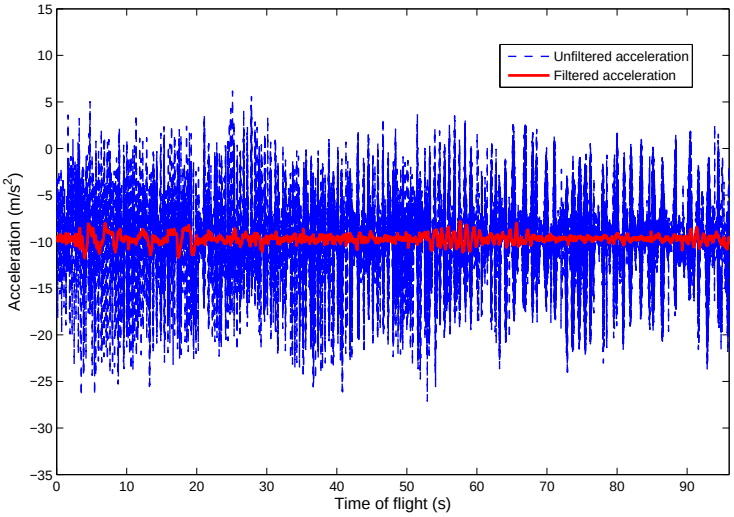

Figure 13. Filtered and unfiltered accelerations

heave motion dynamics in a gusty environment and measurable signals from aboard equipment, an effective gust estimator is developed. In addition, a feedback-feedforward control architecture is presented to stabilize heave motion. Simulation results demonstrate that the proposed gust estimator exhibits satisfactory estimation performance. Moreover, flight tests have justified the feasibility of the proposed control strategy when random gusts occur, which proves its suitability for use in ship-helicopter flight operations.

Appendix A. Parameters of Eagle helicopter

The geometry and aerodynamic parameters of Eagle helicopter are given in Table A.1.

References

[1] Kang, H., He, C., Carico, D.. Modeling and simulation of rotor engagement and disengagement during shipboard operations. In: the

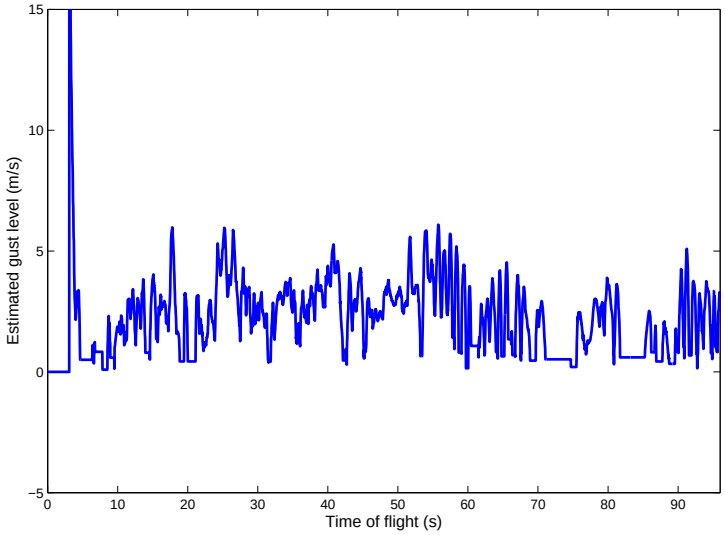

Figure 14. Estimated gusts in the flight test

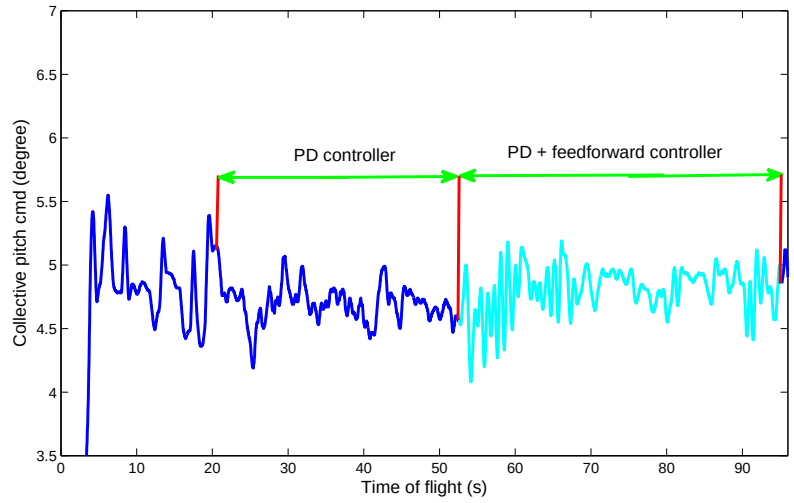

Figure 15. Collective pitch signals (degree)

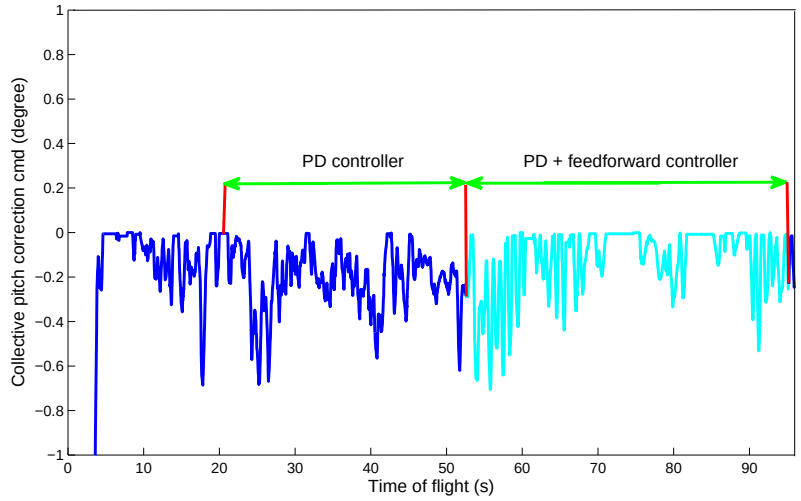

Figure 16. Collective pitch correction signals (degree)

Table A.1. Parameters of Eagle helicopter

Parameters	Description	Value
a	Main rotor blade 2D lift curve slope	5.7
ρ	Air density	1.225 kg/m^3
A_l	Lateral cyclic to main rotor pitch ratio	-0.17 rad/ms
B_l	Longitudinal cyclic to main rotor pitch ratio	-0.19 rad/ms
C_l	Longitudinal cyclic to flybar pitch ratio	-1.58 rad/ms
D_l	Lateral cyclic to flybar pitch ratio	-1.02 rad/ms
c_{mr}	Main rotor blade chord	0.058 m
c_{tr}	Tail rotor blade chord	0.026 m
I_{xx}	Moment of inertia about $x-$axis	0.30 kgm^2
I_{yy}	Moment of inertia about $y-$axis	0.82 kgm^2
I_{zz}	Moment of inertia about $z-$axis	0.40 kgm^2
I_{xz}	Product of inertia	-0.01 kgm^2
S^X_{fus}	Fuselage equivalent flat plate area in $x-$direction	0.025 m^2
S^Y_{fus}	Fuselage equivalent flat plate area in $y-$direction	0.084 m^2
S^Z_{fus}	Fuselage equivalent flat plate area in $z-$direction	0.027 m^2
M_a	All-up weight	8.2 kg
N_b	Number of main rotor blades	2
R	Main rotor radius	0.76 m
Ω	Main rotor angular velocity	167.5 rad/sec
Ω_{tr}	Tail rotor angular velocity	884.3 rad/sec

AHS International 60th Annual Forum and Technology. Baltimore, MD; 2004, p. 315–324.

[2] Xin, H., He, C., Lee, J.. Combined finite state rotor wake and panel ship deck models for simulation of helicopter shipboard operations. In: the American Helicopter Society 57th Annual Forum. Washington, DC: the American Helicopter Society International, Inc.; 2001, p. 1187–1200.

[3] Toffoletto, R., Reddy, R., Lewis, J.. Effect of ship frontal shape variation on flow field in flight deck region. In: Proceedings of the 2nd International Conference on Computational Fluid Dynamics, ICCFD. Sydney, Australia; 2002,.

[4] Fang, R., Booij, P.J.A.. Helicopter-ship qualification testing. American Helicopter Society 62nd Annual Forum 2006;:743–763.

[5] Roper, D.M., Owen, I., Padfield, G.D.. Integrating CFD and piloted simulation to quantify ship-helicopter operating limits. the Aeronautical Journal 2006;(419-428).

[6] Steven, J.H., Steven, J.Z., David, R.M., Gareth, P.D., Ieuan, O.. Time-accurate ship airwake and unsteady aerodynamic loads modeling for maritime helicopter simulation. Journal of American Helicopter Society 2009;54(022005):1–16.

[7] Lee, D., Uzol, N.S., Horn, J.F., Long, L.N.. Simulation of helicopter shipboard launch and recovery with time-accurate airwakes. In: the American Helicopter Society 59th Annual Forum; vol. 1. Phoenix, Arizona: the American Helicopter Society; 2003, p. 1113–1131.

[8] Min, Z., Chang, C., Siang, S.C., Yong, L.N., Jacqueline, S.Z.Q., Adrian, W.T.B.. Analytical approach to helicopter-ship certification. In: the American Helicopter Society 60th Annual Forum; vol. 1. Baltimore, MD: the American Helicopter Society International, Inc.; 2004, p. 257–268.

[9] Turner, G., Clark, W., Cox, I., Finlay, B., Duncan, J.. Project saif-assessment of ship helicopter operating limits using the merlin helicopter simulator. In: the American Helicopter Society 62nd Annual Forum; vol. 1. Phoenix, Arizona: the American Helicopter Society International, Inc.; 2006, p. 226–235.

[10] Kang, H., He, C., Saberi, H.. Dynamic interface simulation of rotorcraft shipboard on-deck operation. In: the American Helicopter Society 59th Annual Forum; vol. 1. Phoenix, AZ: the American Helicopter Society International, Inc.; 2003, p. 1089–1100.

[11] Aouf, N., Boulet, B., Botez, R.. Robust gust load alleviation for a flexible aircraft. Canadian Aeronautics and Space Journal 2000;46:131–140.

[12] Buffington, J.M., Yeh, H.H., Banda, S.S.. Robust control design for an aircraft gust attenuation problem. Proceedings of the 31st IEEE Conference on Decision and Control 1987;:560–561.

[13] Jackson, S., Tisdale, J., Kamgarpour, M., Basso, B., Hedrick, J.K.. Tracking controllers for small uavs with wind disturbances: Theory and flight results. Proceedings of the 47th IEEE Conference on Decision and Control 2008;:564–569.

[14] Cheviron, T., Plestan, F., Chriette, A.. A robust guidance and control scheme of an autonomous scale helicopter in presence of wind gusts. International Journal of Control 2009;82(12):2206–2220.

[15] Martini, A., Leonard, F., Abba, G.. Dynamic modelling and stability analysis of model-scale helicopters under wind gust. Journal of Robot System 2008;.

[16] Garratt, M.A., Ahmed, B., Pota, H.R.. Platform enhancements and system identification for control of an unmanned helicopter. 9th International Conference on Control, Automation, Robotics and Vision 2006;:1981–1986.

[17] Samal, M.K.. Neural network based identification and control of an unmanned helicopter. Ph.D. thesis; University of New South Wales, Australia; 2009.

[18] Ahmed, B., Pota, H., Garratt, M.. Flight control of a rotary wing UAV using backstepping. International Journal of Robust and Nonlinear Control 2009;20(6):639–658.

[19] Garratt, M.A.. Biologically inspired vision and control for an autonomous flying vehicle. Ph.D. thesis; Australian National University, Australia; 2007.

[20] Garratt, M.A., Pota, H.R., Lambert, A., Maslin, S.E.. Systems for automated launch and recovery of an unmanned aerial vehicle from ships at sea. Proceedings of the 22nd International UAV Systems Conference 2007;:1401–1415.

[21] Heffley, R.K., Mnich, M.A.. Minimum-complexity helicopter simulation math model program. Tech. Rep.; U. S. Army Aeroflight Dynamics Directorate, Ames Research Center; 1986.

[22] Bramwell, A.R.S., Done, G., Balmford, D.. Helicopter Dynamics 2nd edition. Butterworth-Heinemann; 2001.

[23] Seddon, J.. Basic Helicopter Aerodynamics. Blackwell Science Ltd.; 1990.

[24] Bramwell, A.R.S.. Helicopter Dynamics. Halsted Press; 1976.

[25] Press, W.H., Teukolsky, S.A., Vetterling, W.T., Flannery, B.P.. Numerical Recipes in C: The Art of Scientific Computing, 2nd ed. Cambridge University Press; 1992.

[26] Flying qualities of piloted aircraft *MIL-F-8785C. Tech. Rep.; United States Department of Defence; 1980.*

[27] Meteorology, A.B.. Australian capital territory weather and warnings 2010;.